

# Strength Optimization of Nanocomposite Cementitious Materials Using Nanoscale Modifications

Arpita Das<sup>1</sup>, Rajdip Paul<sup>2\*</sup>, Showmen Saha<sup>1</sup>

<sup>1</sup> Department of Civil Engineering, Faculty of Civil Engineering, National Institute of Technology Durgapur, Mahatma Gandhi Avenue, Durgapur 713209, India

<sup>2</sup> Department of Civil Engineering, School of Engineering and Technology, Central University of Jharkhand, Ratu-Lohardaga Road, Brambe, Ranchi 835205, India

\* Corresponding author, e-mail: [rajdip.paul@cuja.ac.in](mailto:rajdip.paul@cuja.ac.in)

Received: 02 June 2023, Accepted: 07 January 2024, Published online: 11 March 2024

## Abstract

Represent Volume Element (RVE) is broadly used by investigators to control the properties of nano-cementitious materials. This paper focuses on analyzing a set of RVE data and proposes parametric equations for determining the compressive and flexural strength characteristics ( $\sigma_c$  and  $\sigma_f$ ). Primarily, a parametric study is performed with RVE analysis. The essential design parameters are used to fit rational equations. The RVE data are also applied to train artificial neural networks of  $\sigma_c$  and  $\sigma_f$ . RVE, neural networks, and rational equations are correlated. Regression equations are validated with the experimental study. SEM, TEM, XRD, and FTIR results are carried out in the microscopic and mechanical analysis for carbon nanofiber cement composites, which can lift their strength, constancy, integrity, and density and reinforce the composite microstructure. Lastly, the Pareto-optimal design results are presented with a multi-objective optimization problem.

## Keywords

nanocementitious material, artificial neural network (ANN), optimization, parametric equations, microscopic and mechanical analysis

## 1 Introduction

The use of cement and cementitious materials in construction is very widespread nowadays. However, the tensile strength of Concrete is very much low. Therefore, it is required to provide some reinforcement to enhance flexural strength, ductility, and toughness. Not only that, the nanofibers are used as an energy-saving material. With the addition of some nanofibers in building materials, the buildings are going to be more durable and economical. The tensile strength of the beam is increased using a carbon nanotube (CNT) as a micro reinforcement [1]. The damping capacity is improved using CNT. As a result, CNT-reinforced cement composite carries the dynamic load. The porosity of nano-cementitious material also plays an essential role in increasing the beam composite's vibrational frequencies [2]. As the CNT-reinforced cement composite can absorb the vibration frequency, many researchers also used this composite in the foundation. Zhang et al. [3] analyzed the wave propagation with different shear deformation beam theory in CNT cement composites. Mangalasseri et al. [4] described the energy

harvesting behavior of smart composites like magneto-electro-elastic material with CNT. The investigation shows that electromagnetic circuits influence the nonlinear frequency ratio and give a clear idea about boundary conditions, CNT volume fractions, and geometrical parameters such as aspect ratio and length-to-width ratio [4]. Arshid et al. [5] investigate CNT reinforcement to increase the stiffness of the face sheet of a three-layer sandwich structure, and the mechanical property improves due to CNTs' volume fraction elevation. The experimental investigation of nano cementitious material is a time-consuming and uneconomic procedure. Some analytical models and equations are generated to know the compressive strength of nano silica concrete [6]. CNT polymeric composites are also used in doubly curved micro-shell panels in elastic foundations. These shells express a hardening response under critical buckling of spherical panels [7]. Heidari et al. [8] investigate nanotube's waviness, pristine, and aggregation behavior. Alimirzaei et al. [9] described a nonlinear viscoelastic boron nitride nanotube

micro-composite beam behaviour. The stiffness of the beam increases with an increase in geometrical imperfection parameters, and nonlinear frequency is reduced.

In this paper, some analytical simulation has been done to reduce the cost and number of trials. Numerically, the mechanical properties of CNT-reinforced cement are found by RVE modeling [9]. RVE is the smallest volume over which a measurement can be made to yield an expected value of the whole. In this paper, the property of nanofiber cementitious material is determined by ANSYS 15.0 with the concept of 3D Representative Volume Element (RVE). The cost of nanofibers is relatively higher, but their strength is much higher than other reinforcing materials. Carbon nanofibers (CNF) are rapidly becoming most popular cementitious materials. Alkali-activated slag-type concrete increases the compressive strength of Concrete, but in this paper, tensile strength also increases with CNF in Portland cement [10]. The analytical simulation is also effective in understanding the behavior of nanofiber cementitious material [11–14]. It is used to improve mechanical properties and the rheological properties of asphalt binder mixes in pavement materials [15]. It has excellent mechanical, electrical, and thermal conductivity. CNF can be transmitted into various materials, i.e., elastomers, ceramics, thermoplastics, and thermosets. Introducing nanofiber in a concrete beam without a stirrup can resist crack propagation [16]. Optimization is a unique technique determining the design parameter under a certain operating condition. In 2007, Le et al. [17] optimized the mixing proportion of ultra-high-performance fiber-reinforced Concrete and found the optimum percentage. This paper also finds the optimum percentage of CNF cementitious material. In 2020, Li et al. [18] also used the optimization technique to obtain the property of fresh and hardened ultra-high-performance concrete. The nanofibers or polymer application in different surfaces facilitates modifying the various surface techniques. Carbon nanofibers are made of graphene and can be dispersed in isotropic and anisotropic solutions. The interlaminar region of carbon nanofibers improves the properties of composites for different applications. The chemical vapour deposition of carbon nanofibers is produced by Vapour-grown carbon fiber (VGCNF), from which the nanofiber dispersion, alignment, bond between nanofibre and polymer, and mechanical properties are described by Al-Saleh and Sundararaj [19]. VGCNF had excellent mechanical properties. The thermal stability is very high, giving high strength and ductility in high temperatures and reducing the crack

if clay is coated with CNF composite [20]. According to Zhou et al. [21] in 2009, the electrospun polyacrylonitrile nanofibers consist of phosphoric acid, which enhances the thermal, mechanical, and morphological properties of graphitic carbon nanofibers. This type of graphitic carbon nanofiber is used in the stabilization process. The thermal and mechanical stability is also high, and mechanical stability comes from the microporous ceramic structure of CNF. In the case of morphological property, the best growth of CNF is achieved when an essential amount of nickel nitrate hexahydrate  $\text{Ni}(\text{NO}_3)_2 \cdot 6\text{H}_2\text{O}$  is mixed with a small quantity of acetone [22]. The mechanical stability of CNF is raised by internal walls built by the microporous ceramic structure. This ceramic structure also helps to produce porous material. Carbon nanostructures with porous ceramic internal walls are produced to determine a growth of pore size around 25  $\mu\text{m}$ . There are two steps. First, the nanostructure transfers inside the scaffold. The chemical vapour of nanofibre is deposited into the scaffold using an iron catalyst, and the growing process starts. After the growth process, the catalyst remains in the framework. Walter et al. [23] investigated scaffolds made with alumina, which helps nanofiber growth under the scaffold. Nanofibers are also used as a cementitious material to improve performance and save energy. Scalisi [24], in 2009, used nanofibers as a less energy conservator; as a result, insulation or lighting of a new or old type of building without damage to any building. Some fibers are also secondhand as heat insulation polyurethane foam. Nikje et al. [25], in 2008, also described achieving the best dispersion condition for 3-aminopropyltriethoxysilane (APTS) to be used as a coupling agent, and the use of its thermal, mechanical, and dynamic behavior is going to be enhanced. Mejdoub et al. [26] described Thermal, mechanical, and microstructural properties when nano-fibrillated cellulose is cast off in nano reinforcement in Portland cement. To increase processability, good dispersion stability is required. For that, the resultant hybrid composites are tested, showing that the CNF is much lesser than the electrochemical-specific capacitance of the CNF [27]. As per Ahmed et al. [28], from 400 °C to 570 °C, nanofibers' surface area increased with the potential. This study uses TEM results to determine the sonication time, but these examinations also confirmed that shorter CNFs are more stable than longer ones. TEM also analyses bamboo-like herringbone composite structures where CNF has grown vertically. To investigate XRD results, many researchers considered the Segal equation.

Based on the Segal equation, the crystallinity index of the cellulose nanofiber with diameters 50 to 100 nm is a 72% crystallinity index. Cellulose nanofiber has higher thermal stability than lignin, which is associated with the high crystallinity of CNF [29]. First, the material dried and got into a powder form for an XRD result, and then the other properties like temperature, acid concentration, and mechanical treatment are formed. After getting all properties, crystallinity and *d*-spacing are found. Fourier transform infrared (FTIR) spectroscopy is also custom in this paper to ascertain the chemical properties of nanomaterials and cement matrix. This spectroscopy analysis requires qualitative and quantitative analysis to recognize materials' functional groups. The chemical bonds of functional groups absorbed the infrared energy at particular frequencies. At specific spectral positions, the infrared energy confirms the strength of the material.

The above-conferred studies discussed the properties of various types of carbon nanofiber and how CNF dispersed in solutions and resisted crack propagation using coating by nanofiber. Although the researchers introduce enhancement of mechanical properties, there are many research gaps. Firstly, there was no command concerning two variables, i.e., water-cement ratio and percentage of nanofiber. In this paper, two regression equations are generated, which reduce the design time at the time of strength calculation. In this present study, an optimization technique is considered to get suitable strength and Pareto-optimal design. Secondly, the experimental investigation defines the proper process technique, sonication time-related problems, simulation validation with various models for proper bonding, and consistent improvement of properties. Thirdly, the microscopic physical parameters, i.e., phase-identification, crystalline size, crystallinity index, and *d*-spacing, must be utilized to explain their effect on carbon nanofiber cementitious material. Fourthly, the chemical behavior, i.e., peak values IR response, observed the functional group's electron delocalization. From the past research gaps, the present study aims to establish an essential understanding between CNF and cementitious material with variable percentages of CNF. The study report is blended with the mechanical, chemical, and physical behavior of the CNF cementitious material.

## 2 Materials

This study used Portland cement of grade II to prepare the experimental model. To know the chemical composition of cement, IS 8112:2013 [30] and for Physical characteristics, IS 4031 [31] are used, respectively. Table 1

**Table 1** Properties of cement

|                                      | Oxide component                      | Wight percentage |
|--------------------------------------|--------------------------------------|------------------|
| Chemical component                   | Calcium oxide                        | 63.28            |
|                                      | Silica dioxide                       | 20.22            |
|                                      | Aluminum oxide                       | 4.9              |
|                                      | Iron oxide                           | 3.3              |
|                                      | Sodium oxide                         | 0.98             |
|                                      | Magnesium oxide                      | 2.1              |
|                                      | Sulphuric anhydride                  | 1.6              |
|                                      | Insoluble residue                    | 0.2              |
|                                      | Loss on ignition                     | 1.6              |
|                                      | Chloride content                     | 0.01             |
|                                      | Alkali content                       | 0.008            |
|                                      | Tricalcium aluminate content         | 7.41             |
|                                      | Tricalcium silicate                  | 63.4376          |
| Dicalcium silicate                   | 16.2                                 |                  |
| Physical property                    | Characteristics                      |                  |
|                                      | Fineness m <sup>2</sup> /kg          | 290              |
|                                      | Normal consistency (%)               | 32               |
|                                      | Specific gravity                     | 2.87             |
|                                      | Initial setting time (min)           | 112              |
|                                      | Final setting time (min)             | 240              |
|                                      | Compressive strength 72 ± 1 h (MPa)  | 12               |
|                                      | Compressive strength 168 ± 2 h (MPa) | 23               |
| Compressive strength 672 ± 4 h (MPa) | 36                                   |                  |
| Soundness by autoclave               | 0.8                                  |                  |

describes the chemical and Physical components of the cement. A graphitized (iron-free) composed of conical platelets CNF is considered in this study, which has an average diameter of 130 nm and length varies from 20 μm to 200 m. It is an iron-free content having a pore size of 0.075 cm<sup>3</sup>/g of the average pore volume. The cement and CNF are not the same dimensions, so they are not immersed in water only by hand mix. Due to the various graphitic and compatible properties, the CNF dispersed in the isotropic and anisotropic matrix. The graphitized CNF is dispersed into water by using some superplasticizers. N, N-Dimethylformamide (DMF) is used to disperse the CNF in a cement matrix with a minimum time. After being dispersed into the solution, the pH value of dispersion water is observed. The carbon nanofibers' properties are described in Table 2, taken from Sigma-Aldrich.

## 3 Analytical method

### 3.1 RVE modeling

As the experiment cost is high to decrease the cost of examination and trial, some simulations are carried out by ANSYS 15.0 with the concept of 3D Represent Volume

**Table 2** Properties of carbon nanofibers

| Parameter                     | Specification            |
|-------------------------------|--------------------------|
| Diameter ( $D$ )              | 100 nm                   |
| Length ( $L$ )                | 30 $\mu\text{m}$         |
| Avg dia                       | 130 nm                   |
| Average specific surface area | 24 $\text{m}^2/\text{g}$ |
| Average bulk density          | 2 lb/cu. ft              |
| Purity                        | >90 wt%                  |

Element (RVE) [32]. In this RVE model, the CNF is added to the cementitious material with multiple percentages (0 to 0.5%) by the weight of the cement. There are three types of RVE models. The square RVE model is introduced in this study as per Fig. 1 (b). A simple random sampling is described, i.e., hexagonal RVE, square RVE, and cylindrical RVE (Fig. 1 (a)) [33]. As per Li et al. [18], an array of the nanofiber marked the RVE model, i.e., for the hexagonal array, hexagonal RVE, and the square display, square RVE, as introduced. The cylindrical RVE decreases the simulation work time under any loading system exerted to select the key points in the design. Based on the water-cement ratio and percentage of nanofiber, 148 design points

are selected, as shown in Fig. 1 (c), subsequently creating 148 RVE models. In this paper, the square RVE model is adopted, and after analyzing the model, the stress and load behavior of nanofiber cementitious material is observed. A comparative study is followed to form a regression equation. This paper will first employ the square RVE to estimate the mechanical properties of the CNF-based compounds. Here, the size of the RVE model is considered  $850 \text{ nm} \times 850 \text{ nm}$ . The length of the RVE model is  $5 \mu\text{m}$  as per Table 3. Different models having the exact dimensions giving the various percentages of CNF by weight of cement have been established. It is presumed that the CNFs are uniformly distributed over the entire cementitious model.

The boundary condition is a pinned joint at both ends, and the loads act at the beam's midpoint. This model is endangered to an axial distance  $\Delta L$  at the loading point. Both CNF and cement are displayed using 3-D solid elements in the ANSYS workbench. The property of CNF is obtained from sigma-aldrich.com. Some nonlinear analyses are done as cementitious material is poor in tension and crushed in compression. When modeling, an eight-noded element with proper boundary conditions is considered.

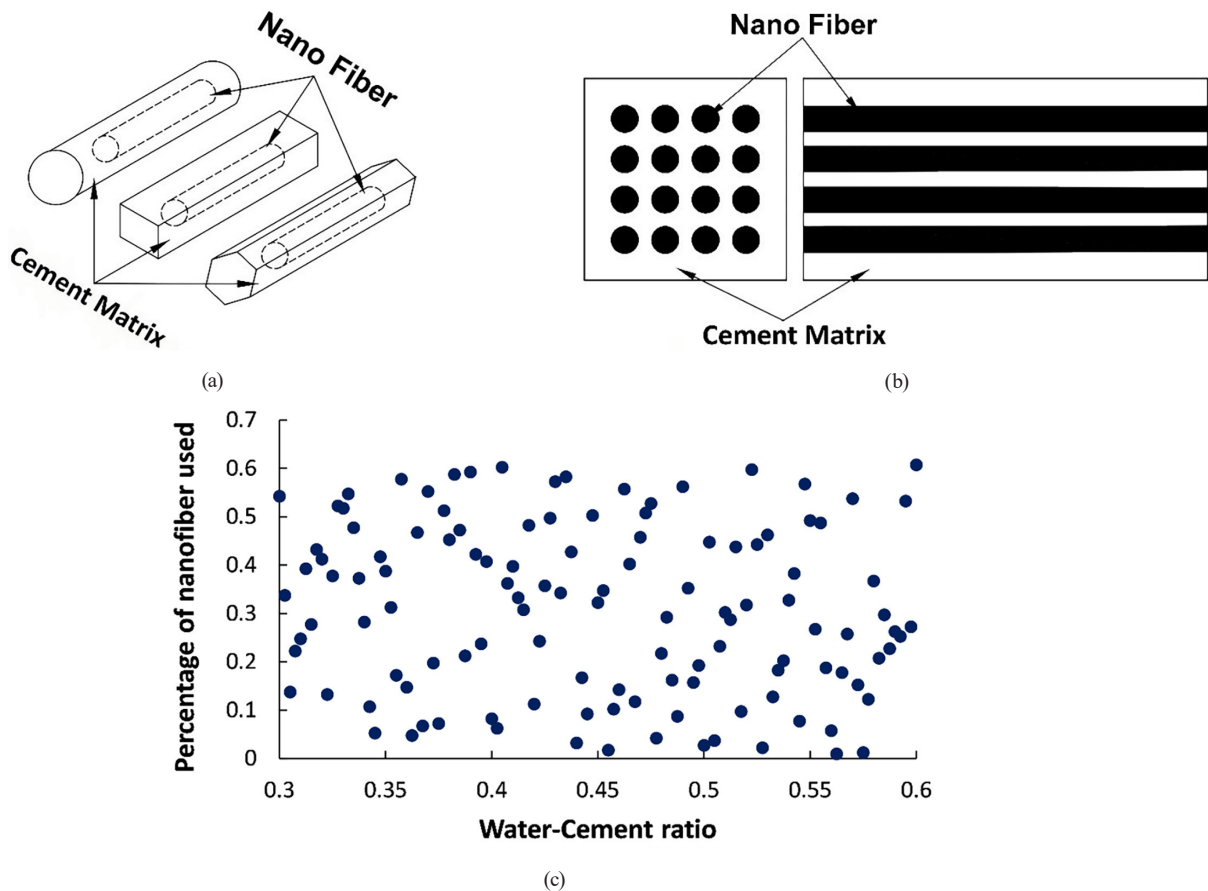


**Fig. 1** (a) Types of the RVE model, (b) representation of RVE in cement composites, (c) design points from random sampling technique

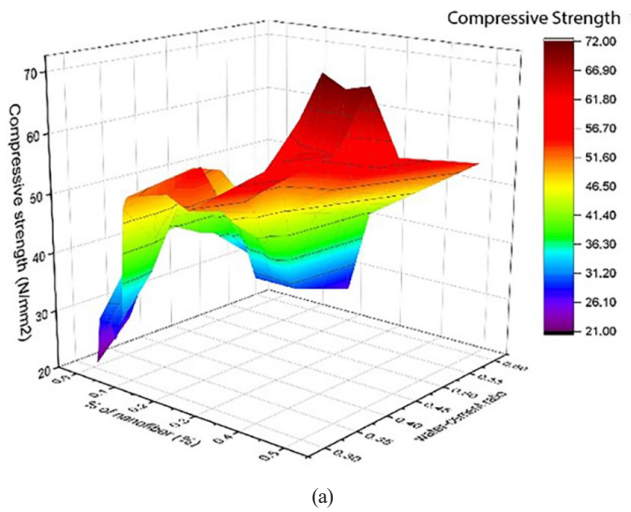
**Table 3** Specification of the RVE model

| Parameter                                  | Specification |
|--|---------------|
| Width and height of the model ( <i>a</i> ) | 850 nm        |
| Length of the model ( <i>L</i> )           | 10 μm         |
| The outer diameter of CNF                  | 130 nm        |
| The thickness of CNF                       | 60 nm         |
| The inner diameter of CNF                  | 70 nm         |

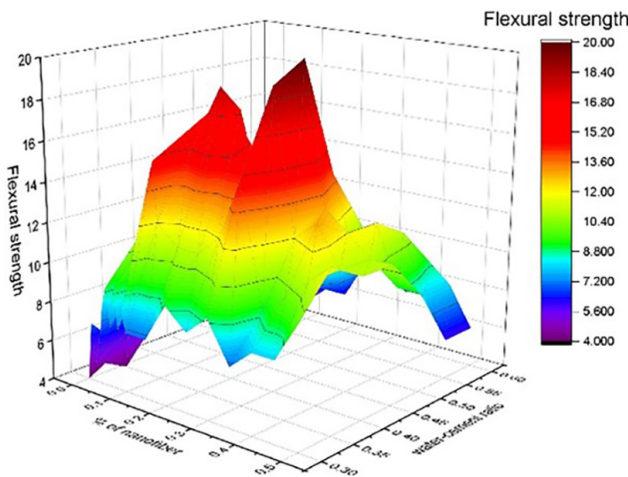
Fig. 2 represents the surface plot of the compressive as well as the tensile strength of 148 design points concerning two design functions: water-cement ratio and percentage of nanofiber.

The assumptions of this element are as follows:

- The material is supposed to be primarily isotropic
- At each amalgamation point, cracking is allowed in three orthogonal directions
- If any cracking occurs at an amalgamation point, it is simulated by altering material properties. These discrete cracks are treated as a tarnished band of cracks.



(a)



(b)

**Fig. 2** Function values at 148 design points (a)  $\sigma_c$ , (b)  $\sigma_f$

### 3.2 Regression equation

As discussed earlier, the mechanical properties, i.e., the compressive and flexural strength of various nano cementitious materials, are obtained from the RVE model at the design points. A parametric assessment for mortar under thermal loading is generated by Raoufi et al. [34]. In Fig. 2, the function values are plotted at every design point. The RVE results are utilized to generate another model in Systat Table Curve 3D for fitting a nonlinear curve [35]. Levenburg–Marquardt algorithm is considered for minimizing the mean square error function fitting. The RVE results of compressive and flexural strength are integrated into regression equations with the excellent bonding of the forms. The RVE results of compressive strength ( $\sigma_c$ ) and flexural strength ( $\sigma_f$ ) are tailored to the forms of the rational equations,

$$\sigma_c = \frac{a_1 + a_2x + a_3x^2 + a_4y}{1 + b_1x + b_2y + b_3y^2} \quad (1)$$

$$\sigma_f = \frac{a_1 + a_2x + a_3y + a_4y^2 + a_5y^3}{1 + b_1x + b_2y} \quad (2)$$

where *x* represents the water-cement ratio, and *y* represents the percentage of nanofibre. Table 4 and Table 5 present the  $\sigma_c$ ,  $\sigma_f$  coefficients, and  $R^2$ . The  $R^2$  means standard error, and the values of  $R^2$  are more significant than 0.92, which represents outstanding for generating an analytical model.

**Table 4** Coefficients  $a_i$  and  $b_i$  for the regression equation of  $\sigma_c$  with standard error and the  $R^2$  value

| Coefficient | Value | Standard error | $R^2$      |
|-------------|-------|----------------|------------|
| $a_1$       | 25    | 0.020797953    |            |
| $a_2$       | 17    | 0.012456357    |            |
| $a_3$       | -18   | 0.007553467    |            |
| $a_4$       | 83    | 0.563434326    | 0.98236618 |
| $b_1$       | 1     | 0.123436521    |            |
| $b_2$       | -0.2  | 0.013412655    |            |
| $b_3$       | -3.3  | 0.000676542    |            |

**Table 5** Coefficients  $a_i$  and  $b_i$  for the regression equation of  $\sigma_f$  with standard error and the  $R^2$  value

| Coefficient | Value | Standard error | $R^2$     |
|-------------|-------|----------------|-----------|
| $a_1$       | 1     | 0.049779946    |           |
| $a_2$       | 70    | 0.037653487    |           |
| $a_3$       | 115   | 0.002364318    |           |
| $a_4$       | 10    | 0.096452675    | 0.9433562 |
| $a_5$       | -15   | 0.006353565    |           |
| $b_1$       | 1     | 0.164575557    |           |
| $b_2$       | -0.07 | 0.035423576    |           |

Three-dimensional plots of the parametric equations of  $\sigma_c$  and  $\sigma_f$  are shown in Fig. 3 (a) and (b), respectively.

### 3.3 Artificial Neural Networks

Artificial neural networks (ANN) are very popular among researchers nowadays. After creating the regression equations of  $\sigma_c$  and  $\sigma_f$ , ANN is to accomplish a more consistent study. Many researchers carried out ANN in the civil engineering field to expand the neural net, i.e., Charrier and Ouellet-Plamondon [35] presented ANN for slump and dynamic analysis with a proper mixture proportion of admixture. Analysis and design of large structures under the neural net of various propagation. ANN is adopted to optimize numerical and structural neurocomputing strategies [36]. Backpropagation of ANN is used to design a double-layer grid [37]. Fuzzy neural networks (FNN) are built to identify the patterns of mean pressure distribution [38]. Optimize the transmission tower's design and

develop a robust simulation-based optimization ANN prepared for analysis and design of the surrogate model [39]. Fig. 4 represents a feedforward backpropagation network for nanocomposite material.

#### 3.3.1 Algorithm of artificial neural network

Researchers considered the selection of algorithms, architecture networks, patterns, and neuron numbers taken as rational numbers for selecting the appropriate size and topography of the neural network. Not only is it used in the strength characteristic of cementitious material, but it is also used to obtain the force coefficient of wind load concerning tall structures [40]. Minor errors occur if the training pattern response is not suitable. Hunter et al. [41] proposed many training designs and minimum neurons for less error. In this study, multilayer perceptron (MLP) architecture (feedforward backpropagation) and the Levenberg–Marquardt (LM) algorithm are used.

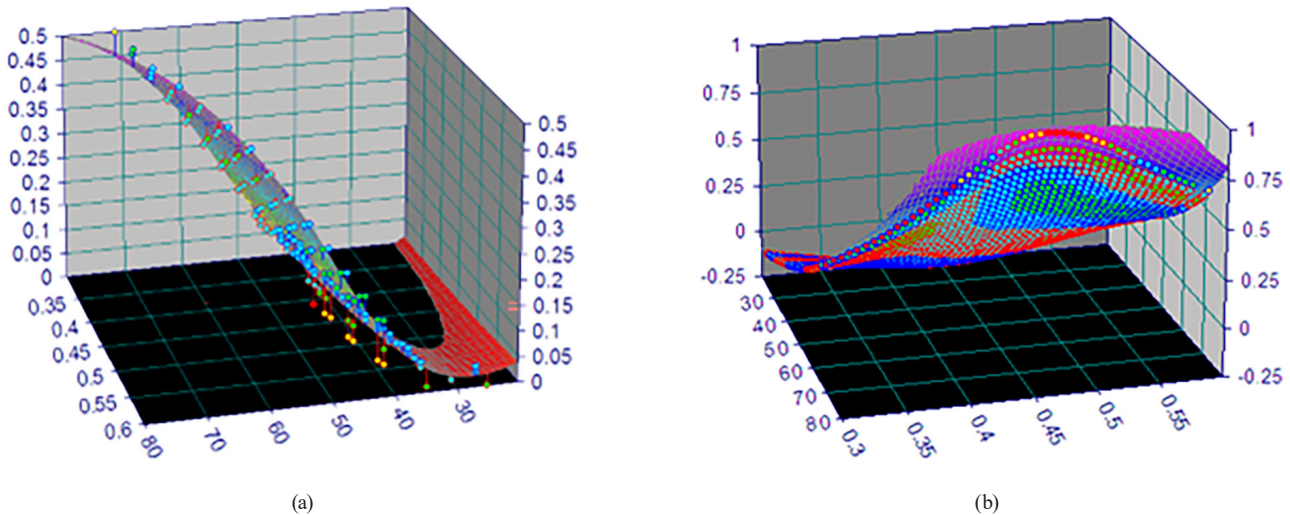


Fig. 3 Surface plots of the regression equations of the strength as a function of  $x$  (water-cement ratio) and  $y$  (percentage of nanofibre) (a)  $\sigma_c$ , (b)  $\sigma_f$

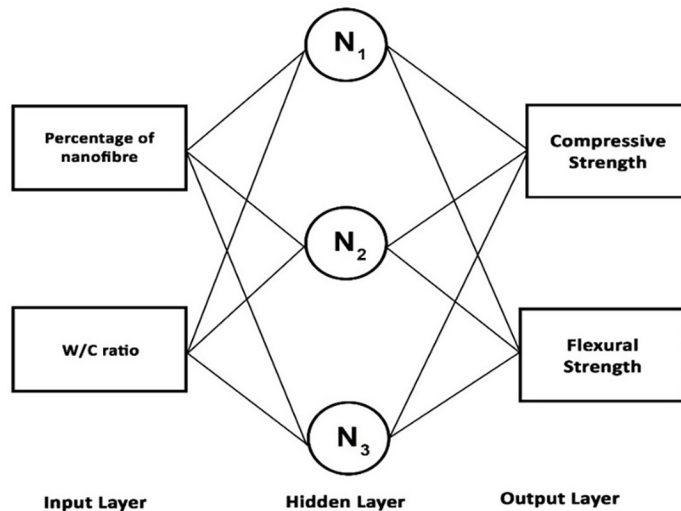


Fig. 4 FFBP network for nanofiber cementitious material

The network architecture adopted in this study is shown in Fig. 5. Levenberg [42] describes multiple second-order methods for the neural network, and among these methods, the LM algorithm is taken in these most efficient studies [42–44]. As per Hagan and Menhaj [44], the trained MLP network architecture is only solved by this algorithm with a small problem. Here, the feedforward backpropagation (FFBP) network is chosen for the neural network. Fig. 5 characterizes the FFBP network flow chart [44].

### 3.3.2 The target of the neural network

The flowchart demonstrates the expansion of the FFBP of the neural network model. The error histogram lessened in every case to retain the target value closer to the output value. The present study contains one input and hidden layer with three neurons and one output layer in the ANN. The regression value varies from 0 to 1, indicating the relationship quality between output and targets. Here, the ANN is obtained with 350 epochs and incrementally increases with 50 unless the desired degree of accuracy is achieved. The histogram shows the error with 20 bins representing the bar width of 0.00411. The error histogram for ANN of  $\sigma_c$  and  $\sigma_f$  is shown in Fig. 6. From the graph, it is observed the error percentage in most of the cases is 0.2%. The error percentage is justified as it is small and under the specific percentage or water-cement ratio.

### 4 Comparison results of RVE, ANN, and parametric equations

The mechanical properties of nano cementitious material are achieved at individual design points from RVE, regression equation, and ANN. Fig. 7 represents compressive strength ( $\sigma_c$ ), and Fig. 8 represents the flexural strength ( $\sigma_f$ ) at each design point. The comparative result shows that the results from RVE models match the effects of both RVE and ANN. The higher error percentage in the compressive strength results obtained from the RVE model, ANN, and regression equation is limited to 2% at most design points. Still, an occasional higher percentage error is observed in flexural strength results. Fig. 4 shows that the results fluctuate when the water-cement ratio increases after 0.5. After increasing the water-cement ratio greater than 5, increasing the percentage of nanofiber does not increase its mechanical properties. Within this region of the water-cement ratio, the surrogate model predicts a higher flexural strength value than RVE and ANN's results. In the case of higher prediction values, the effect of stresses is not threatening from the structural safety point of view. An effective conclusion from Figs. 7 and 8 predicts the mechanical property responses of nanofiber cementitious material. The structure and Algorithm utilized to train the networks can be suitably accepted to conduct similar studies.

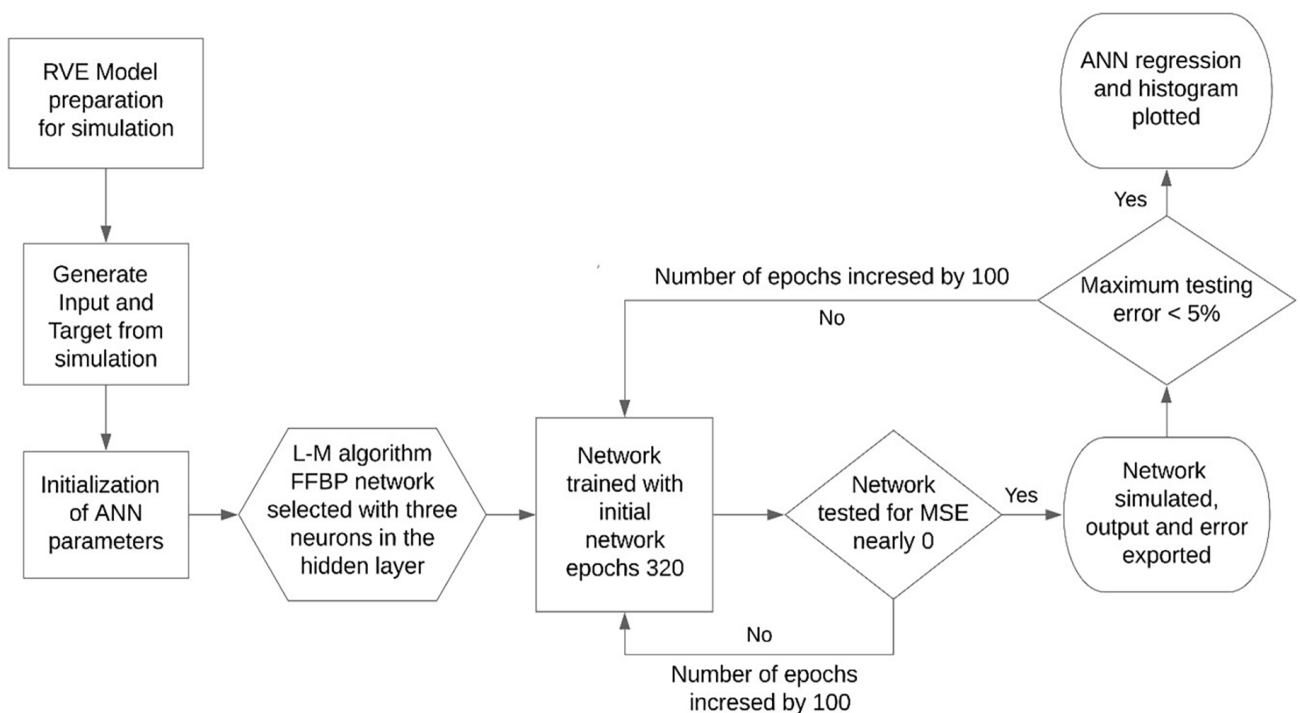


Fig. 5 The flowchart for the development of the FFBP network

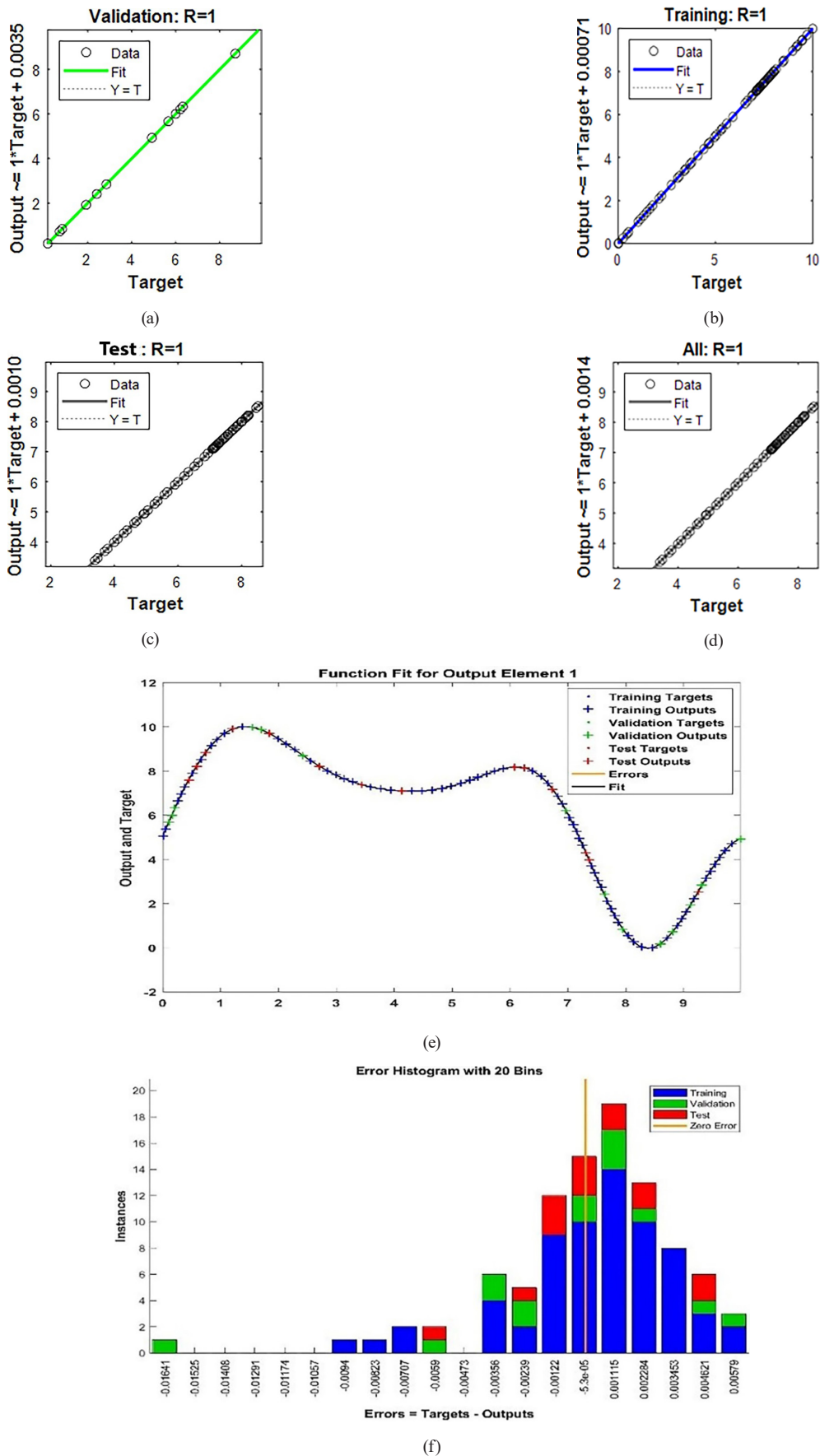


Fig. 6 Regression plots for (a) Validation, (b) Training, (c) Test, (d) All, (e) Training target and output element and (f) Error Histogram developed of ANN model (single hidden layer)

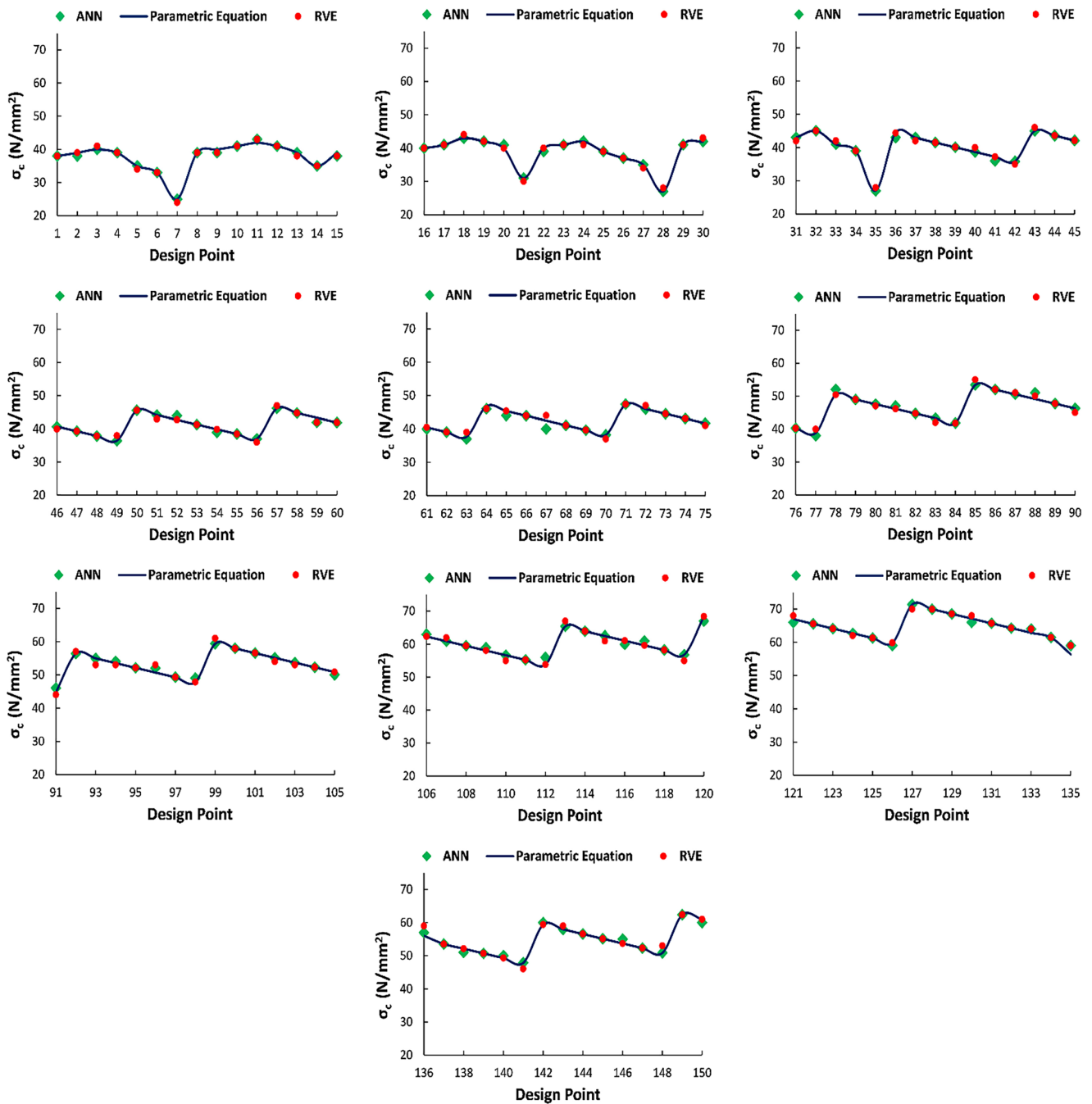


Fig. 7 Comparative plot of compressive strength achieved from RVE, parametric equation, and ANN at all the design points

### 5 Experimental method

After getting the regression equation, it is validated with some experimental work. For that, twenty-four beams and cubes are cast in this study. The beam specimen dimensions, the corresponding water-cement ratio, and the percentage of CNF are considered as per Table 6. In every set, three number beams are cast for the 3-point flexure bending strength test, and three cubes (50 mm × 50 mm × 50 mm) are cast for the compressive strength test. As per Yazdani

and Mohanam [45], in 2016, and Tyson et al. [46], in 2011 N, N-dimethyl formaldehyde is used to mix with water where the surfactant-to-water ratio is 0.005 [45, 46]. An aqueous solution is prepared by mixing water, surfactant, and CNF. A pH meter measured the aqueous solution's pH, ranging from 8.2 to 8.4. After measuring the pH value, the solution is sonicated for 30 min by an ultrasonic sonicator (model F.S. – 750, frequency 23 ± 3 KHz), as shown in Fig. 9.

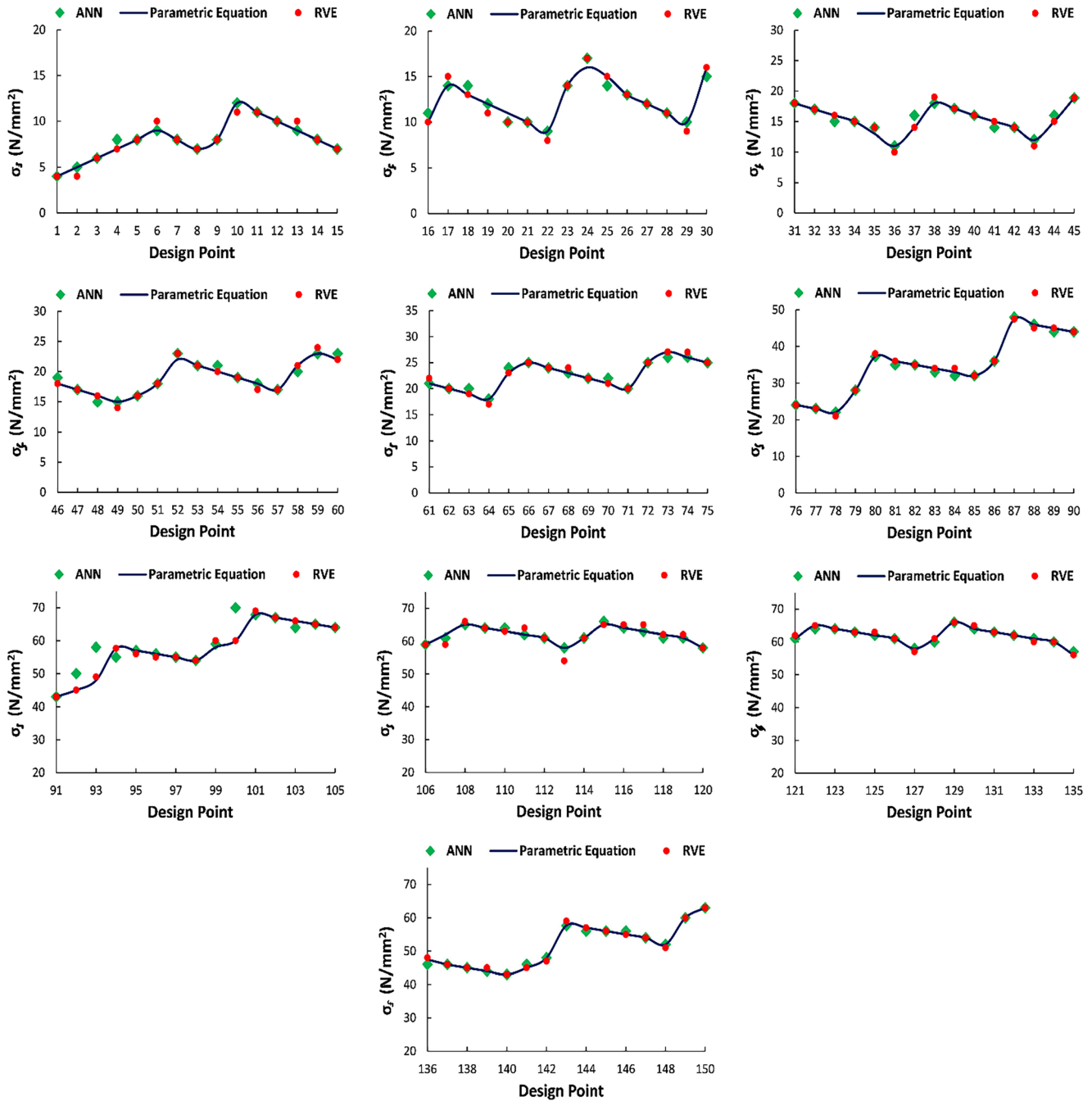


Fig. 8 Comparative plot of flexural strength achieved from RVE, parametric equation, and ANN at all the design points

Table 6 Description of beam specimen

| Specimen title | Specimen description   | Water-cement ratio | Percentage of CNF |
|----------------|------------------------|--------------------|-------------------|
| SET 1          | 400 mm × 14 mm × 14 mm | 0.4                | 0                 |
| SET 2          | 400 mm × 14 mm × 14 mm | 0.4                | 0.2               |
| SET 3          | 400 mm × 14 mm × 14 mm | 0.4                | 0.3               |
| SET 4          | 400 mm × 14 mm × 14 mm | 0.4                | 0.4               |

The sonicated time is dependent upon the TEM result. After 15 min sonication, some black spots are visible in the TEM results. By improving sonication time, i.e., 30 min, the black spots on the sample are removed. After sonication,

the dispersed solution is mixed with cementitious material. A multispeed planetary mixer is used for 13 to 18 min to increase the evenness of the matrix. Before moulding, the even sample is rest 4 to 6 min in a vacuum chamber to



(a)



(b)



(c)

Fig. 9 (a) Sonication by ultrasonic sonicator; (b) cube sample;  
(c) beam specimen

remove the air bubbles. After that, the sample is placed in wooden moulds with a cross-section of  $14 \text{ mm} \times 14 \text{ mm}$  and also poured into the cube mould with a dimension of  $50 \text{ mm} \times 50 \text{ mm} \times 50 \text{ mm}$ , as shown in Fig. 9. An electric surface vibrator is used to fill the embedded air voids. All samples are de-moulded after twenty-four hours and kept in saturated lime water for curing for 28 days. X-ray

diffraction patterns are also considered here. A Miniflex Desktop X-ray Diffractometer Rigaku, with a Cu Target and having radiation at 30 kV and 15 mA. The Scanning Range is  $\sim 30 \sim +1500$  ( $2\theta$ ), and the Scanning speed is  $0.010 \sim 1000/\text{min}$ . After 28 days, some powder sample is prepared for each type set for the XRD result.

In this paper, some samples are prepared to investigate the SEM image. Very thin specimens of all samples are prepared, and after coating with silver wrapping, the samples are placed in a Scanning electron microscope. This paper used the Shimadzu Irprestige-21 model (installed in CMERI Durgapur) for diffuse reflectance spectroscopy. The scan range of this model is  $400 \text{ nm} - 4000 \text{ nm}$  Wave Length- $\text{nm}^{-1}$ . The technique is utilized here per Fuller and Griffiths's description of diffuse reflectance. The sample is scanned with  $2.0 \text{ cm}^{-1}$  resolution, and the average data is presented. The sample is prepared and analyzed three times, and the average of these three is considered to minimize differences due to sample preparation. After preparation, the sample is sent to the DR-FTIR spectrometer test.

### 5.1 Experimental setup

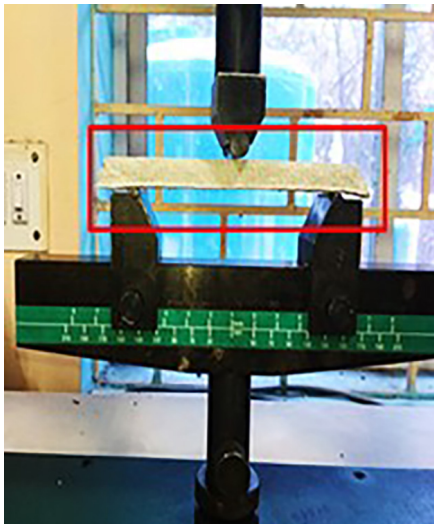
In this study, two types of specimens: one cube specimen for conducting the compression strength test and another beam specimen for conducting the flexural (3-point bending strength) test. The compression test is done by a Universal Testing Machine made by HEICO, shown in Fig. 10. The flexural strength test is done by a three-point bending strength test machine (H50KS by Tinue Olesen) installed in CMERI Durgapur, shown in Fig. 10. An Excel sheet is prepared from the test results. From the strength of material relation, these data are converted to stress-strain,

i.e., stress  $\sigma = \frac{3pL}{2bd^2}$  and  $\epsilon = \frac{6Dd}{L^2}$ , where  $p$  is the force

from a load cell,  $L$  = span length [45] [here, beam length = 400 mm],  $b$  = width,  $d$  = depth is  $14 \text{ mm} \times 14 \text{ mm}$ , and  $D$  is the corresponding displacement. Scanning Electron Microscopic (SEM) results are taken for every sample to observe the bonding properties between cement paste and CNF. To follow the surface crack of the sample, a Scanning Electron Microscope (S-3000N) with a high resolution is used. A fracture surface is cut approximately  $3 \times 3 \times 1 \text{ mm}$  from every set of samples for the SEM sample, and a three nm thick palladium layer is coated with the surface to enhance surface conductivity. Suppose the coating is not implemented to the surface of the SEM sample. In that case, the results or image could not be generated because the cement is not a conductive material, so the electron has not reached the surface of the materials.



(a)



(b)



(c)

**Fig. 10** (a) Setup H50KS by Tinu Olesen, (b) 3-point bending, (c) compression strength testing machine

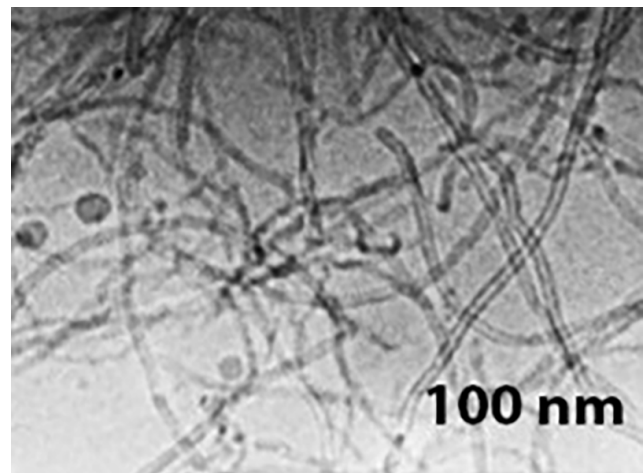
## 6 Result and discussion

### 6.1 Aqueous solution

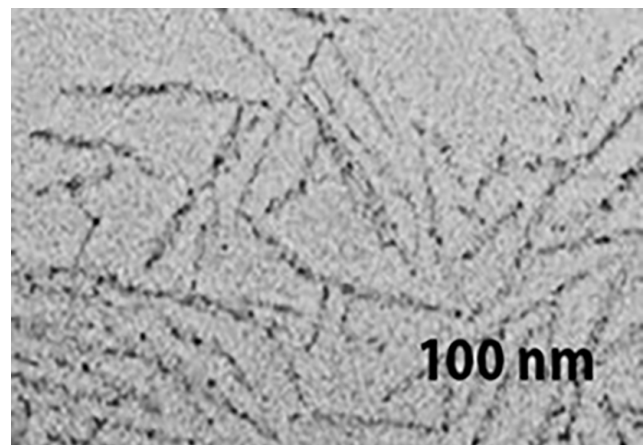
A transmission Electron Microscope image is considered for the different sample types to determine the sonicated time in the ultrasonic mixture and whether it is dispersed correctly or not. In Fig. 11, the sonication is done for 15 min. After 30 min, sonication with 1.25% surfactant by water weight gives better results, and all-black spots are removed.

### 6.2 Mechanical properties

Flexural strength and compressive strength are done for 7, 14, and 28 days to find out the mechanical properties. The size of the cube mould and the water-cement ratio as described in Table 3. The peak load is considered for the compression strength test, and a bar chart is followed as per Fig. 12 (a). Here, the bar represents the peak value of compressive strength with time. Fig. 12 (b) shows that CNF improves the peak load and peak displacement of

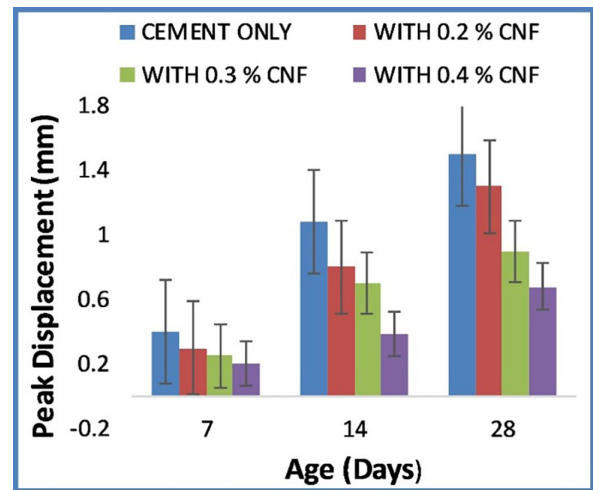
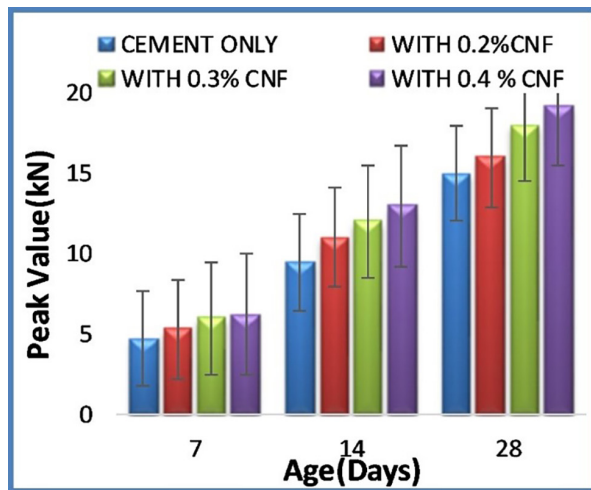


(a)



(b)

**Fig. 11** Dispersion of CNF in aqueous solution after (a) 15 min, (b) 30 min sonication



(a) (b)  
 Fig. 12 Effect of (a) peak load and (b) peak displacement with or without CNF

cement paste at first, but at a certain percentage, the peak displacement is decreased with an increase of CNF % with cement. It is also observed that the increase in strength is minor for increasing nano filament for compressive strength. Eight sets of the beam are cast for bending strength, and after 7, 14, and 28 days, the 3-point bending strength results are observed. As the ultimate strength gains in 28 days, bending strength results are considered for 28 days. The results are shown in Fig. 13. In this study, it is observed that an increase of nanofibre up to 0.3% increased the strength (set 1 to set 3), and for set 4, the bending strength decreased. As a result, the bending strength increases to a certain percentage but decreases afterward. The elastic modulus of various sets of cementitious material also increases with the proportion of carbon nanofibers. Using MATLAB 2022a, the toughness is found out from the stress-strain curve. In the case of toughness, the curve is increasing, but after a certain percentage, it will descend in order.

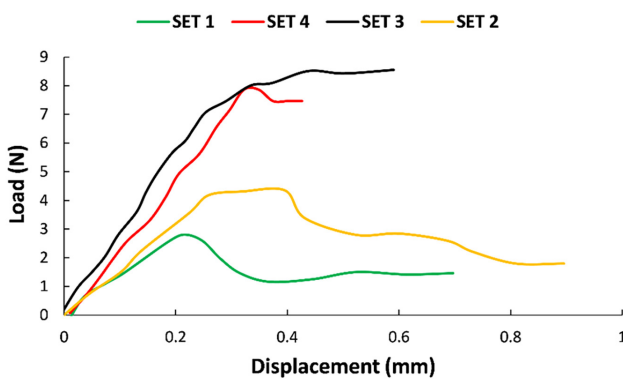


Fig. 13 Load displacement response of 3-point bending strength at 28 days

### 6.3 Regression equations validation with the experimental results

Optimization studies are used to pronounce the exactness of the substitute models. Experimental studies are also done to validate analytical studies. As mentioned above, three types of percentages with a fixed water-cement ratio are prepared for the experimental study. The results are shown in Table 7. It detected that, for  $\sigma_c$  and  $\sigma_f$ , the inconsistency percentage is below 10% except for 0.4% carbon nanofiber cementitious material as it seems to be an over-reinforced material.

### 6.4 Validation of equation with the publish data

The surrogate model is again validated for nanofiber cementitious material. The mechanical properties of nano cementitious material are compared with the results published by Das et al. [12–14]. For the percentage (0.04%, 0.08%, and 0.1% nanofiber) of cementitious material, the comparisons are presented in Table 8. For both  $\sigma_c$  and  $\sigma_f$ , the inconsistent error percentage is 0.01.

### 6.5 Optimization results

Optimization work has been conceded to apprehend the effect of nanofiber in cementitious material. Firstly, numerical optimization of the mechanical property  $\sigma_c$  and  $\sigma_f$  is directed by single objectives. When a specific percentage of nanofiber oversees the water-cement ratio, suitable results are obtained. The analysis of minimization and maximization is done using a genetic algorithm technique with two design variables,  $x$  and  $y$ . In optimization analysis, 200 generations are considered the maximum number.

**Table 7** Comparison of the values of the  $\sigma_c$  and  $\sigma_f$  of various percentages of nanofiber

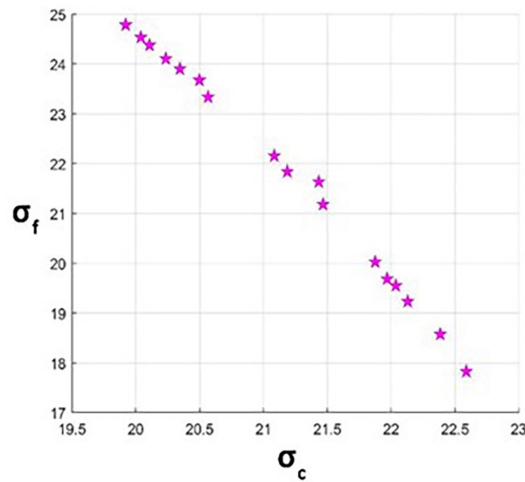
| Mechanical property | 0.2% CNF cementitious material |                     | 0.3% CNF cementitious material |                     | 0.4% CNF cementitious material |                     |
|---------------------|--------------------------------|---------------------|--------------------------------|---------------------|--------------------------------|---------------------|
|                     | Experimental work              | Regression equation | Experimental work              | Regression equation | Experimental work              | Regression equation |
| $\sigma_c$          | 52                             | 50                  | 59                             | 58                  | 78                             | 82                  |
| $\sigma_f$          | 36                             | 37                  | 47                             | 45                  | 51                             | 56                  |

**Table 8** Comparison of the values of the  $\sigma_c$  and  $\sigma_f$  of various percentages of nanofiber

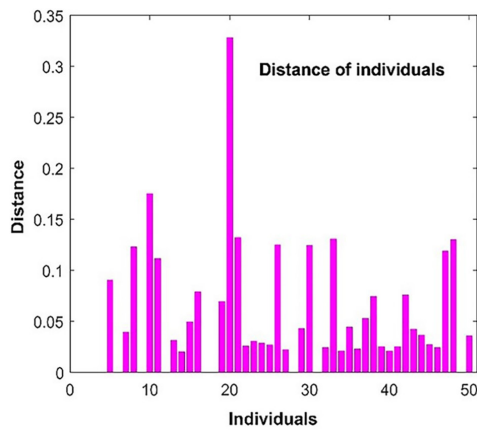
| Mechanical property | 0.04% CNF cementitious material |                     | 0.08% CNF cementitious material |                     | 0.1% CNF cementitious material |                     |
|---------------------|---------------------------------|---------------------|---------------------------------|---------------------|--------------------------------|---------------------|
|                     | Das et al. [12–14]              | Parametric equation | Das et al. [12–14]              | Parametric equation | Das et al. [12–14]             | Parametric equation |
| $\sigma_c$          | 44                              | 45                  | 46                              | 46                  | 49                             | 48                  |
| $\sigma_f$          | 24                              | 24                  | 25                              | 27                  | 32                             | 31                  |

The minimum value of  $\sigma_c$  is 41, achieved for  $x = 0.4$  mm and  $y = 0.3$ . For  $\sigma_f$ , the least value is obtained at  $x = 0.6$  and at  $y = 0.01$ . The minimum value of  $\sigma_f$  is obtained as 24. The critical result of  $\sigma_c$  is 207, and the  $x$  and  $y$  values are 0.4 mm and 0.45, respectively. For  $\sigma_f$ , the extreme value is obtained at  $x = 0.4$  and  $y = 0.3$ . Lastly, a multi-objective optimization analysis (MOGA) is done concerning RVE

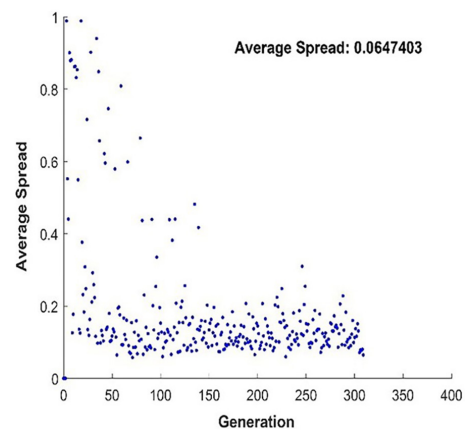
models to minimize and maximize the mechanical characteristics of nano-cementitious material  $\sigma_c$  and  $\sigma_f$ . In the MOGA toolbox of MATLAB, the regression equation is put as input functions. In this study, 200 generations are considered for global Pareto-optimal Solutions, and the design results are shown in Fig. 14 (a). As this solution gives better output than the other design space solution, 18 candidates



(a)



(b)



(c)

**Fig. 14** Pareto optimal solutions for the MOGA analysis (a) pareto front; (b) pareto distance; (c) average pareto spread

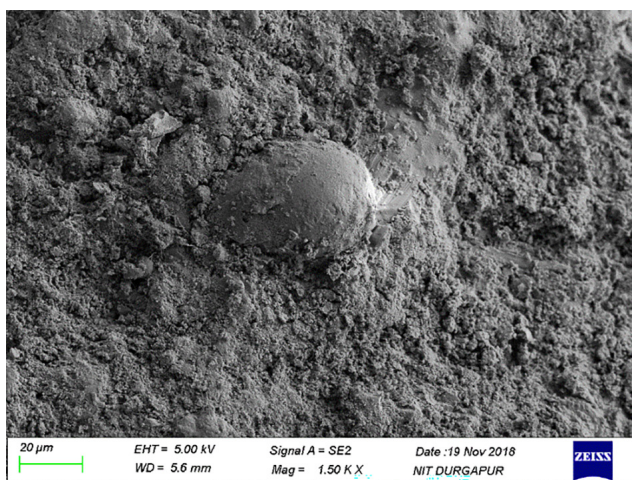
of the Pareto front are observed to achieve the strength shown in Fig. 14 (a). Fig. 14 (b) represents the statistical information about the Pareto distance. The average Pareto spread is plotted in Fig. 14 (c), representing individuals' distance measure change concerning the previous generation.

### 6.6 SEM observation

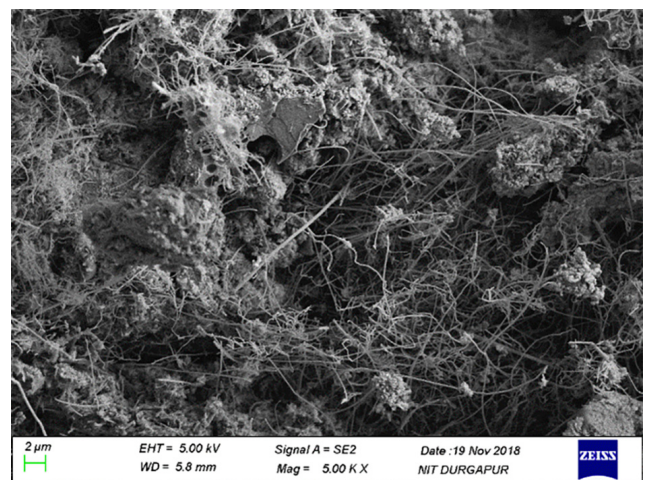
The TEM result is observed to know the proper mixing of nanofiber in an aqueous solution, but after blending up the solution with the cement matrix, poor dispersion is shown in SEM results. Fig. 15 (a) shows that the lumps are generated when the aqueous solution is mixed with the cement matrix by hand mixing, and when it is mixed with a multispeed planetary mixer with 0.2% CNF, the lumps are removed (Fig. 15 (b)). After enlarging the SEM image, it is observed that a microcrack is generated (Fig. 15 (c)) in a specific region where the concentration of CNF is

present. It happened due to the weak binding of CNF in a cement matrix. At the time of hydration, after hardening the cement, hydrate the outer edge of the surface.

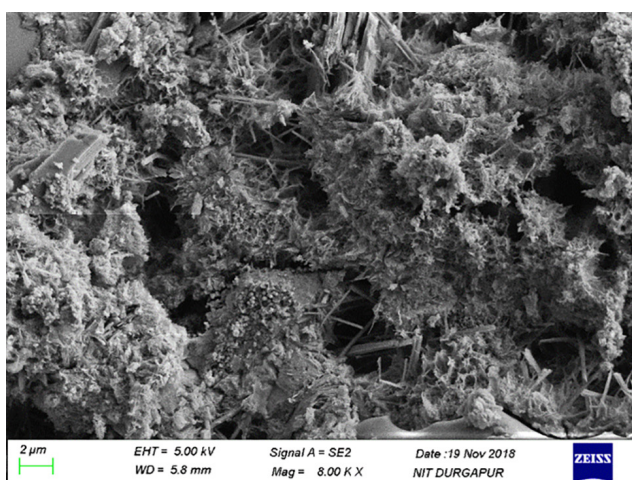
The grains hydrated without CNF and prepared C-S-H without any CNF. When the CNF is present, the areas are much more significant than individual cement grains. In that case, the cement is clumped together, and as a result, cracks are generated. The dispersion of cementitious material is described by Everts et al. [47]. Here, in Fig. 15 (c), the microcrack is generated, and the presence of carbon nanofibers tried to pull them out. Fig. 15 (d) shows a micro crack pulled out by CNF, i.e., other surfaces pulled one surface, and it is widespread in SEM images. Due to untreated nano filament having a smooth surface, the bond strength is not generated properly. As a result, due to the weaker bond, some microcracks are not resolved to increase the percentage of CNF.



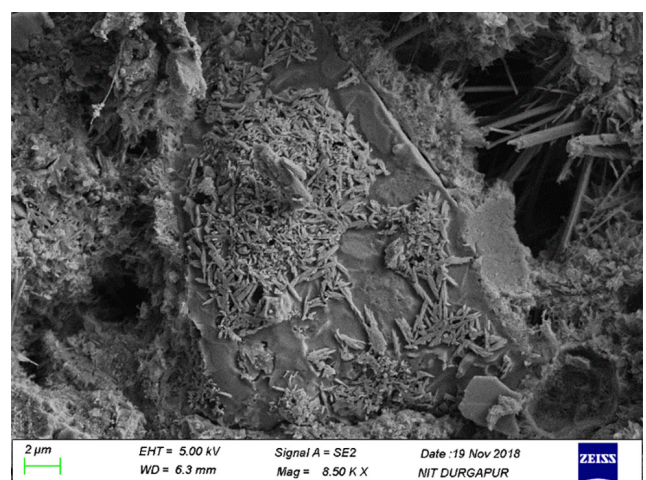
(a)



(b)



(c)



(d)

**Fig. 15** SEM image of CNF cementitious material using (a) hand mixing, (b) a multispeed planetary mixer, (c) micro cracked fractured surface, (d) pulled out from a microcrack

**6.7 XRD results**

XRD results are performed for all samples to investigate phase identification. The dried powder from all models is prepared for the XRD analysis. Fig. 16 shows the corresponding diffraction pattern of cementitious material. Hydration products also showed, including SiO<sub>2</sub> and CaCO<sub>3</sub>. The SiO<sub>2</sub> and, CaCO<sub>3</sub>, and CNF data matched with 26.7019, 29.475, 30.217, 43.005, based on JCPDS, respectively. JCPDS match software is introduced, and the sample powder diffraction phase is identified. Fig. 16 displays that crystalline graphite interlayer in 2θ = 20–50°. In the case of cement, there some changes occurred, and this interlayer 2θ = 25–48°. XRD diffraction results of the cement sample are shown in Fig. 16. For the cement sample, it can be easily stated that the number of peaks is turned less than cement with the nanofiber sample, and here, match data coincided with the reference data at 26.67, 34.33 and 46.77. This indicated that the presence of carbon layers increases the number of peaks and the value of 2-theta, revealing encapsulated iron. After Analysis of XRD peak profiles of cement and CNF cementitious materials, it can be said that the FWHM means full-width at half-maximum and is also effective for measuring sensitiveness in stress-strain built-up and microstructure in the material. Here, the FWHM value of CNF increases

more rapidly than the FWHM values of cement. As per Sahli et al. [48], a Linear decrease of FWHM in the XRD peak represents an increase in density and hardness and a decrease in the crystallinity. The XRD pattern of CNF cementitious material and cement is shown in Fig. 16. Using the Scherrer equation, the crystallite size is calculated from XRD graphs [49].

$$L_{h,k,l} = \frac{K\lambda}{\beta \cos \theta} \tag{3}$$

In Eq. (3), K = 0.9 and λ = 1.5418 Å based on the FWHM value of 101 and 002 reflections. The crystallinity percentage is also calculated using Eq. (4).

$$\% \text{ Crystallinity} = \frac{I_{002} - I_{am}}{I_{002}} \times 100 \tag{4}$$

Crystallite size and crystallinity index values for all samples are described in Table 9.

This is based on the perpendicular plane of 002, 101. The Crystallinity of CNF cementitious material is also increased due to the decrease of amorphous fractions. The XRD gives more information on each sample's interlayer of existing elements and graphite. The CNF matched with data JCPDS data. From Fig. 16, it is observed that the d-spacing interlayer of crystalline graphite is not changed in

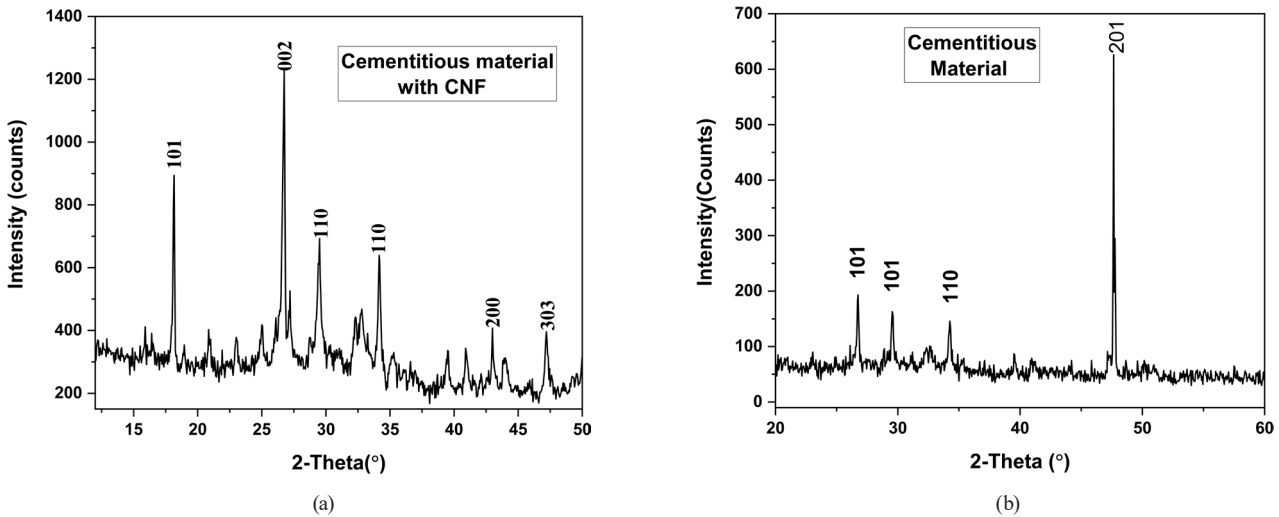


Fig. 16 XRD Peak results for (a) cementitious material with CNF and (b) only cementitious material

Table 9 D-spacing, Crystallinity Index, and crystal size of various sample

| Sample                                  | CNF      | Cementitious material | Cementitious material with 0.1% CNF | Cementitious material with 0.2% CNF | Cementitious material with 0.3% CNF |
|---|----------|-----------------------|-------------------------------------|-------------------------------------|-------------------------------------|
| d-spacing of the plane                  | 0.387    | 0.403                 | 0.393                               | 0.384                               | 0.384                               |
| Crystallinity Index (CI)                | 88       | 56                    | 67                                  | 72                                  | 79                                  |
| Crystal size perpendicular to the plane | 15.57978 | 3.869799181           | 4.888924872                         | 5.266741573                         | 9.747869988                         |

$2\theta = 20\text{--}30^\circ$ . The crystallinity index is increased when the percentage of CNF cementitious material increases as the amorphous phases are present in a regular cement matrix.

### 6.8 FTIR results

Fourier transform infrared (FTIR) analysis results with or without CNF nanocomposite particles are shown in Fig. 17. After preparing a sample, Infrared radiation is absorbed in various wavelengths, generating the molecular composition. Due to a change in the chemical structure, there is a change in the peaks after the heating process. Fig. 17 shows the evolution of the FTIR peak and pattern. In short, since IR is vulnerable to heat, this should be the decomposition of organic components into carbon material. The FTIR peak is changed when the temperature

is higher than  $180^\circ\text{C}$ . The performance of IR response is feeble for carbon materials. Fig. 17 represents the FTIR spectra of the various percentages of cementitious material. The graph reveals the shift of characteristic peaks from  $450\text{ cm}^{-1}$  to  $3800\text{ cm}^{-1}$ . The FT-IR spectra of hardened cement pastes are compared with some percentage of CNF at 28 days of hydration.

The wideband observed in the region  $1355, 2068, 2256,$  and  $2942\text{ cm}^{-1}$  is caused by C-O, the symmetric and irregular stretching of the O-H vibrator of the water molecules. Fig. 17 compares with and without CNF (various percentages) in a cementitious material. The detectable broad peaks of Fig. 17 (a) at  $1115, 1375, 2039, 2278, 2499, 2886,$  and  $3136\text{ cm}^{-1}$  suggest the presence of some organic functional groups, such as C-O, O-H, and carboxyl groups,

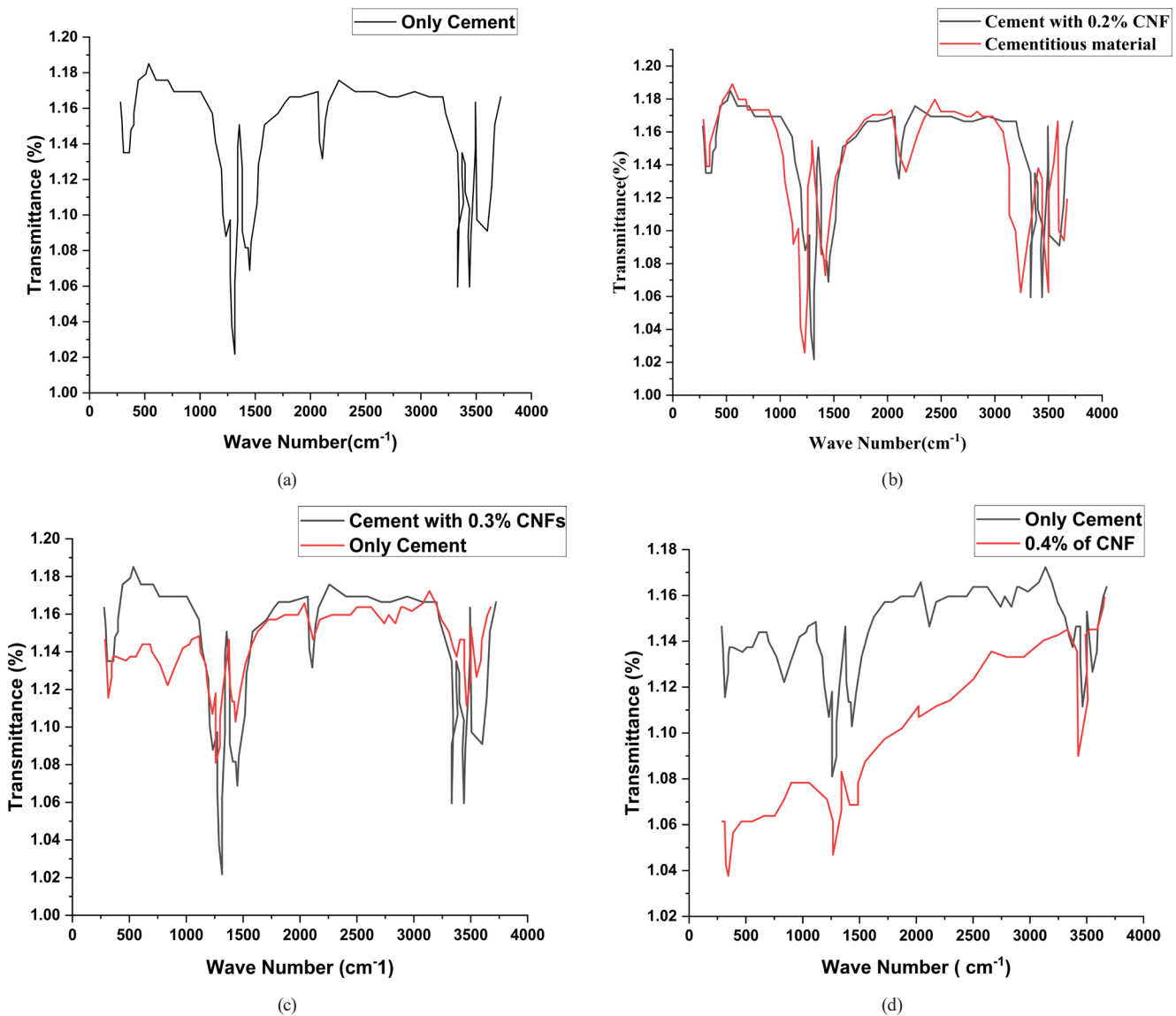


Fig. 17 FTIR graph for (a) cementitious material, (b) cementitious material with 0.2% CNF, (c) cementitious material with 0.3% CNF, (d) cementitious material with 0.4% CNF

which could enable the adsorption of aniline via hydrogen bond. Fig. 17 (b) and Fig. 17 (c) shows the FTIR graph for 0.2% and 0.3% CNF introduced in cementitious material that detects the board peaks of 1352, 1457, 1738, 2194, 2803, and 1340, 2020, 2660 3331, respectively. This peak is correlated with the spectroscopy table, which is attributed to the Benzenoid rings' C=O and C-H stretching vibration mode, the widening mode of C-N, and the protonated C-N group. Fig. 17 (d) also shows that introducing various percentages of CNF gives increasing intensities of most peaks of the cementitious material compared with normal cementitious material. It indicates that polymer adhesion with CNF is good, leading to restricted molecular chain motion. These interactions may enable electron delocalization, increasing bonding between cementitious material and CNF.

## 7 Conclusions

This study focused on determining the optimum water-cement ratio and optimum percentage of nanofiber in CNF-cementitious material. A three-point loading beam structure is considered for preparing the RVE model analysis. The optimization process involves a detailed RVE, parametric equation, and genetic algorithm. The subsequent conclusion can be drawn as presented below:

1. The current study contains regression equations for defining the strength characteristics of a nano-cementitious material with various water-cement ratios that can be gladly accepted for design resolutions.
2. At every design point, ANN calculation for both  $\sigma_c$  and  $\sigma_f$  nearly superimposes the RVE results and regression equations after the ANN trained with the high regression value. This study shows training ANN with an appropriate architecture and algorithm value.

## References

- [1] Madenci, E., Ö., Özkılıç, Y. O., Hakamy, A., Tounsi, A. "Experimental tensile test and micro mechanic investigation on carbon nanotube reinforced carbon fiber composite beams", *Advances in Nano Research*, 14(5), pp. 443–450, 2023. <https://doi.org/10.12989/anr.2023.14.5.443>
- [2] Alsubaie, A. M., Alfaqih, I., Al-Osta, M. A., Tounsi, A., Chikh, A., Mudhaffar, I. M., Tahir, S. "Porosity-dependent vibration investigation of functionally graded carbon nanotube-reinforced composite beam", *Computers and Concrete*, 32(1), pp. 75–85, 2023. <https://doi.org/10.12989/cac.2023.32.1.075>
- [3] Zhang, Y. W., Ding, H. X., She, G. L., Tounsi, A. "Wave propagation of CNTRC beams resting on elastic foundation based on various higher-order beam theories", *Geomechanics and Engineering*, 33(4), pp. 381–391, 2023. <https://doi.org/10.12989/gae.2023.33.4.381>
- [4] Mangalasseri, A. S., Mahesh, V., Mukunda, S., Mahesh, V., Ponnusami, S. A., Harursampath, D., Tounsi, A. "Vibration based energy harvesting performance of magneto-electro-elastic beams reinforced with carbon nanotubes", *Advances in Nano Research*, 14(1), pp. 27–43, 2023.
- [5] Arshid, E., Khorasani, M., Soleimani-Javid, Z., Amir, S., Tounsi, A. "Porosity-dependent vibration analysis of FG microplates embedded by polymeric nanocomposite patches considering hygrothermal effect via an innovative plate theory", *Engineering with Computers*, 38(5), pp. 4051–4072, 2022.
- [6] Garg, A., Aggarwal, P., Aggarwal, Y., Belarbi, M. O., Chalak, H. D., Tounsi, A., Gulia, R. "Machine learning models for predicting the compressive strength of Concrete containing nano silica", *Computers and Concrete*, 30(1), pp. 33–42, 2022. <https://doi.org/10.12989/cac.2022.30.1.033>

It is worth mentioning that the fracture-mechanical characteristics are not discussed in this paper. How the crack growth may be reduced using nanofiber is a future research area. The behavior of CNF-cementitious material with dynamic load and free vibration is also under the future scope of work.

- [7] Huang, Y., Karami, B., Shahsavari, D., Tounsi, A. "Static stability analysis of carbon nanotube reinforced polymeric composite doubly curved micro-shell panels", *Archives of Civil and Mechanical Engineering*, 21(4), 139, 2021.  
<https://doi.org/10.1007/s43452-021-00291-7>
- [8] Heidari, F., Taheri, K., Sheybani, M., Janghorban, M., Tounsi, A. "On the mechanics of nanocomposites reinforced by wavy/defected/aggregated nanotubes", *Steel and Composite Structures*, 38(5), pp. 533–545, 2021.  
<https://doi.org/10.12989/scs.2021.38.5.533>
- [9] Alimirzaei, S., Mohammadimehr, M., Tounsi, A. "Nonlinear analysis of viscoelastic micro-composite beam with geometrical imperfection using FEM: MSGT electro-magneto-elastic bending, buckling and vibration solutions", *Structural Engineering and Mechanics*, 71(5), pp. 485–502, 2019.  
<https://doi.org/10.12989/sem.2019.71.5.485>
- [10] Sindu, B. S., Sasmal, S., Gopinath, S. "Numerical simulation of CNT incorporated cement", *International Journal of Civil and Environmental Engineering*, 6(8), pp. 639–644, 2012.  
<https://doi.org/10.5281/zenodo.1074667>
- [11] Chaparro, W. A., Ruiz, J. H. B., Gómez, R. D. J. T. "Corrosion of Reinforcing Bars Embedded in Alkali-activated Slag Concrete Subjected to Chloride Attack", *Materials Research*, 15(1), pp. 57–62, 2012.  
<https://doi.org/10.1590/S1516-14392011005000096>
- [12] Das, A., Saha, S., Bhowmik, D. "Analytical Simulation of Nanocomposite Cementitious Materials with Carbon Nano Fibers (CNF)", In: *International Conference on Nanotechnology: Ideas, Innovations, and Initiatives-2017 (ICN:3I-2017)*, Roorkee, India, Dec. 6–8, 2017.
- [13] Das, A., Saha, S., Bhowmik, D. "Analytical evaluation of strength attributes for different nanocomposite cementitious materials", In: *11th Structural Engineering Convention – 2018 (SEC-2018)*, Kolkata, India, 2018, 088/R1. ISBN 978-93-83660-46
- [14] Das, A., Saha, S., Bhowmik, D. "Elastic Behavior of Nanocomposite Cementitious Material Using Various Nanopolymer", [pdf] In: *Proceedings of 64th International Congress of ISTAM 9-12, Argul, India, 2019, PID 105*. Available at: [https://istam.iitkgp.ac.in/resources/2019/proceedings/Paper\\_Full/105fullpaper.pdf](https://istam.iitkgp.ac.in/resources/2019/proceedings/Paper_Full/105fullpaper.pdf)
- [15] Amirkhani, A. N., Xiao, F., Amirkhani, S. N. "Characterization of Unaged Asphalt Binder Modified with Carbon Nano Particles", [pdf] *International Journal of Pavement Research and Technology*, 4(5), pp. 281–186, 2011. Available at: [http://www.ijprt.org.tw/mailweb/files/sample/V4N5\(281-286\).pdf](http://www.ijprt.org.tw/mailweb/files/sample/V4N5(281-286).pdf)
- [16] Altoubat, S., A., Yazdanbakhsh, A., Rieder, K.-A. "Shear Behavior of Macro-Synthetic Fiber-Reinforced Concrete Beams without Stirrups", *ACI Materials Journal*, 106(4), pp. 381–389, 2009.  
<https://doi.org/10.14359/56659>
- [17] Le, T. T., Soutsos, M. N., Millard, S. G., Barnett, S. J. "UHPRC-Optimisation of mix proportions: concrete platform", In: *Concrete Platform: An international conference in honour of Professor Adrian Long and Professor John Bungey*, Belfast, United Kingdom, 2007, pp. 339–348.
- [18] Li, P. P., Brouwers, H. J. H., Chen, W., Yu, Q. "Optimization and characterization of high-volume limestone powder in sustainable ultra-high performance concrete", *Construction and Building Materials*, 242, 118112, 2020.  
<https://doi.org/10.1016/j.conbuildmat.2020.118112>
- [19] Al-Saleh, M. H., Sundararaj, U. "A review of vapour grown carbon nanofiber/polymer conductive composites", *Carbon*, 47(1), pp. 2–22, 2009.  
<https://doi.org/10.1016/j.carbon.2008.09.039>
- [20] Gelves, G. A., Al-Saleh, M. H., Sundararaj, U. "Highly electrically conductive and high-performance EMI shielding nanowire/polymer nanocomposites by miscible mixing and precipitation", *Journal of Materials Chemistry*, 21(3), pp. 829–836, 2011.  
<https://doi.org/10.1039/C0JM02546A>
- [21] Zhou, Z., Lai, C., Zhang, L., Qian, Y., Hou, H., Reneker, D. H., Fong, H. "Development of carbon nanofibers from aligned electrospun polyacrylonitrile nanofiber bundles and characterization of their microstructural, electrical, and mechanical properties", *Polymer*, 50(13), pp. 2999–3006, 2009.  
<https://doi.org/10.1016/j.polymer.2009.04.058>
- [22] Muneer, I., Farrukh, M. A., Javaid, S., Shahid, M., Khaleeq-ur-Rahman, M. "Synthesis of Gd<sub>2</sub>O<sub>3</sub>/Sm<sub>2</sub>O<sub>3</sub> nanocomposite via sonication and hydrothermal methods and its optical properties", *Superlattices and Microstructures*, 77, pp. 256–266, 2015.  
<https://doi.org/10.1016/j.spmi.2014.10.006>
- [23] Walter, C., Barg, S., Ni, N., Maher, R. C., García-Tuñón, E., Zaiviji Ismail, M. M., Babot, F., Saiz, E. "A novel approach for the fabrication of carbon nanofibre/ceramic porous structures", *Journal of the European Ceramic Society*, 33(13–14), pp. 2365–2374, 2013.  
<https://doi.org/10.1016/j.jeurceramsoc.2013.04.024>
- [24] Scalisi, F. "Nano-structured Materials in New and Existing Buildings: To Improved Performance and Saving of Energy", In: *Nanotechnology in Construction 3*, Prague, Czech Republic, 2009, pp. 351–356. ISBN 978-3-642-00979-2  
[https://doi.org/10.1007/978-3-642-00980-8\\_47](https://doi.org/10.1007/978-3-642-00980-8_47)
- [25] Nikje, M. M. A., Nikrah, M., Mohammadi, F. H. A. "Microwave-assisted Polyurethane Bond Cleavage via Hydroglycolysis Process at Atmospheric Pressure", *Journal of Cellular Plastics*, 44(5), pp. 367–380, 2008.  
<https://doi.org/10.1177/0021955X08090279>
- [26] Mejdoub, R., Hammi, H., Suñol, J. J., Khitouni, M., M'nif, A., Boufi, S. "Nanofibrillated cellulose as nano reinforcement in Portland cement: Thermal, mechanical and microstructural properties", *Journal of Composite Materials*, 51(17), pp. 2491–2503, 2017.  
<https://doi.org/10.1177/0021998316672090>
- [27] Du, X., Liu, H.-Y., Cai, G., Mai, Y.-W., Baji, A. "Use of facile mechanochemical method to functionalize carbon nanofibers with nanostructured polyaniline and their electrochemical capacitance", *Nanoscale Research Letters*, 7(1), 111, 2012.  
<https://doi.org/10.1186/1556-276X-7-111>

- [28] Ahmed, Y. M., Al-Mamun, A., Jameel, A. T., AlKhatib, M. F. R., Amosa, M. K., AlSaadi, M. A. "Synthesis and Characterization of Carbon Nanofibers Grown on Powdered Activated Carbon", *Journal of Nanotechnology*, 2016, 1538602, 2016.  
<https://doi.org/10.1155/2016/1538602>
- [29] Gea, S., Siregar, A. H., Zaidar, E., Harahap, M., Indrawan, D. P., Perangin-Angin, Y. A. "Isolation and Characterisation of Cellulose Nanofibre and Lignin from Oil Palm Empty Fruit Bunches", *Materials*, 13(10), 2290, 2020.  
<https://doi.org/10.3390/ma13102290>
- [30] BIS "IS 8112:2013 Indian Standard Ordinary Portland Cement, 43 Grade — Specification (Second Revision)", Bureau of Indian Standards, New Delhi, India, 2013.
- [31] BIS "IS 4031 Methods of Physical Tests for Hydraulic Cement (Second Revision)", Bureau of Indian Standards, New Delhi, India, 1996.
- [32] Lichinchi, M., Lenardi, C., Haupt, J., Vitali, R. "Simulation of Berkovich nanoindentation experiments on thin films using finite element method", *Thin Solid Films*, 312(1–2), pp. 240–248, 1998.  
[https://doi.org/10.1016/S0040-6090\(97\)00739-6](https://doi.org/10.1016/S0040-6090(97)00739-6)
- [33] Sindu, B. S., Sasmal, S., Gopinath, S. "Numerical Simulation of CNT Incorporated Cement", *International Journal of Civil and Environmental Engineering*, 6(8), pp. 639–644, 2012. [online] Available at: <https://publications.waset.org/10135/numerical-simulation-of-cnt-incorporated-cement>
- [34] Raoufi, K., Schlitter, J., Bentz, D., Weiss, J. "Parametric Assessment of Stress Development and Cracking in Internally Cured Restrained Mortars Experiencing Autogenous Deformations and Thermal Loading", *Advances in Civil Engineering*, 2011, 870128, 2011.  
<https://doi.org/10.1155/2011/870128>
- [35] Charrier, M., Ouellet-Plamondon, C. M. "Artificial neural network for the prediction of the fresh properties of cementitious materials", *Cement and Concrete Research*, 156, 106761, 2022.  
<https://doi.org/10.1016/j.cemconres.2022.106761>
- [36] Iranmanesh, A., Kaveh, A. "Structural optimization by gradient-based neural networks", *International Journal for Numerical Methods in Engineering*, 46(2), pp. 297–311, 1999.  
[https://doi.org/10.1002/\(SICI\)1097-0207\(19990920\)46:2<297::AID-NME679>3.0.CO;2-C](https://doi.org/10.1002/(SICI)1097-0207(19990920)46:2<297::AID-NME679>3.0.CO;2-C)
- [37] Kaveh, A., Servati, H. "Design of double layer grids using back-propagation neural networks", *Computers & Structures*, 79(17), pp. 1561–1568, 2001.  
[https://doi.org/10.1016/S0045-7949\(01\)00034-7](https://doi.org/10.1016/S0045-7949(01)00034-7)
- [38] Tayfur, G., Erdem, T. K., Kırca, Ö. "Strength Prediction of High-Strength Concrete by Fuzzy Logic and Artificial Neural Networks", *Journal of Materials in Civil Engineering*, 26(11), 04014079, 2014.  
[https://doi.org/10.1061/\(ASCE\)MT.1943-5533.0000985](https://doi.org/10.1061/(ASCE)MT.1943-5533.0000985)
- [39] Kaveh, A., Gholipour, Y., Rahami, H. "Optimal Design of Transmission Towers Using Genetic Algorithm and Neural Networks", *International Journal of Space Structures*, 23(1), pp. 1–19, 2008.  
<https://doi.org/10.1260/02663510878534207>
- [40] Paul, R., Dalui, S. K. "Optimization of alongwind and crosswind force coefficients on a tall building with horizontal limbs using surrogate modeling", *The Structural Design of Tall and Special Buildings*, 30(4), e1830, 2021.  
<https://doi.org/10.1002/tal.1830>
- [41] Hunter, D., Yu, H., Pukish III, M. S., Kolbusz, J., Wilamowski, B. M. "Selection of Proper Neural Network Sizes and Architectures—A Comparative Study", *IEEE Transactions on Industrial Informatics*, 8(2), pp. 228–240, 2012.  
<https://doi.org/10.1109/TII.2012.2187914>
- [42] Levenberg, K. "A method for the solution of certain nonlinear problems in least squares", *Quarterly of Applied Mathematics*, 2(2), pp. 164–168, 1944.  
<https://doi.org/10.1090/qam/10666>
- [43] Marquardt, D. W. "An Algorithm for Least-Squares Estimation of Nonlinear Parameters", *Journal of the Society for Industrial and Applied Mathematics*, 11(2), pp. 431–441, 1963.  
<https://doi.org/10.1137/0111030>
- [44] Hagan, M. T., Menhaj, M. B. "Training feedforward networks with the Marquardt algorithm", *IEEE Transactions on Neural Networks*, 5(6), pp. 989–993, 1994.  
<https://doi.org/10.1109/72.329697>
- [45] Yazdani, N., Mohanam, V. "Carbon Nano-Tube and Nano-Fiber in Cement Mortar: Effect of Dosage Rate and Water-Cement Ratio", *International Journal of Material Science*, 4(2), pp. 45–52, 2014.  
<https://doi.org/10.14355/ijmsci.2014.0402.01>
- [46] Tyson, B. M., Al-Rub, R. K. A., Yazdanbakhsh, A., Grasley, Z. "Carbon Nanotubes and Carbon Nanofibers for Enhancing the Mechanical Properties of Nanocomposite Cementitious Materials", *Journal of Materials in Civil Engineering*, 23(7), 1028, 2011.  
[https://doi.org/10.1061/\(ASCE\)MT.1943-5533.000026](https://doi.org/10.1061/(ASCE)MT.1943-5533.000026)
- [47] Everts, B., Perona-Wright, G., Smits, H. H., Hokke, C. H., van der Ham, A. J., ..., Schramm, G. "Omega-1, a glycoprotein secreted by *Schistosoma mansoni* eggs, drives Th2 responses", *Journal of Experimental Medicine*, 206(8), pp. 1673–1680, 2009.  
<https://doi.org/10.1084/jem.20082460>
- [48] Sahli, J., El Ghardallou, M., Bougmiza, I., Henchiri, B., Limam, M., Mejdoub, R., Mtiraoui, A., Ajmi, T. "Safety evaluation of anticancer drugs circuit in a regional hospital in Tunisia", *The Pan African Medical Journal*, 23, 30, 2016.  
<https://doi.org/10.11604/pamj.2016.23.30.8600>
- [49] Das, K., Tiwari, R. K. S., Shrivastava, D. K. "Techniques for evaluation of medicinal plant products as antimicrobial agent: Current methods and future trends", *Journal of Medicinal Plants Research*, 4(2), pp. 104–111, 2010.  
<https://doi.org/10.5897/JMPR09.030>